REPORT DOCUMENTATION PAGE

Form Approved
OMB NO. 0704-0188

1. AGENCY USE ONLY (Leave Blank)	2. REPORT DATE	3. REPORT TYPE AND DATES COVERED
	9/26/01	Final Progress Report 01Jul98-30Jun01

4. TITLE AND SUBTITLE
A Novel Principle for Data Processing from Hand-Held Ground Penetrating Radars

5. FUNDING NUMBERS
DAAG 55-98-1-0401

6. AUTHOR(S)
Michael V. Klibanov, PI; Thomas R. Lucas, Co-PI

7. PERFORMING ORGANIZATION NAME(S) AND ADDRESS(ES)
University of North Carolina at Charlotte
9201 University City Boulevard, Charlotte, NC 28223

8. PERFORMING ORGANIZATION REPORT NUMBER

9. SPONSORING / MONITORING AGENCY NAME(S) AND ADDRESS(ES)
U. S. Army Research Office
P.O. Box 12211
Research Triangle Park, NC 27709-2211

10. SPONSORING / MONITORING AGENCY REPORT NUMBER
ARO Proposal No. 38897~~-MA-LMD~~ .8-C1-LMD

11. SUPPLEMENTARY NOTES
The views, opinions and/or findings contained in this report are those of the author(s) and should not be construed as an official Department of the Army position, policy or decision, unless so designated by other documentation.

12 a. DISTRIBUTION / AVAILABILITY STATEMENT
Approved for public release; distribution unlimited.

12 b. DISTRIBUTION CODE

13. ABSTRACT (Maximum 200 words)

The goal of this project was to develop a new algorithm of inverse problems to image locations and electrical properties of land mines using GPR data. These parameters, in turn, might be used on a next stage as an input for the classification procedure. Such a method has been developed and tested on models. Accurate images of mine-like targets are demonstrated. Comparison with the best competing algorithm in the field favors the algorithm of this project. The main innovation, as compared with conventional algorithms is the differential rather than conventional integral form of the resulting system. This enables one to obtain solutions in a much shorter time, as compared with the conventional techniques.

14. SUBJECT TERMS	15. NUMBER OF PAGES 34
	16. PRICE CODE

17. SECURITY CLASSIFICATION OR REPORT	18. SECURITY CLASSIFICATION ON THIS PAGE	19. SECURITY CLASSIFICATION OF ABSTRACT	20. LIMITATION OF ABSTRACT
UNCLASSIFIED	UNCLASSIFIED	UNCLASSIFIED	UL

NSN 7540-01-280-5500

Standard Form 298 (Rev.2-89)
Prescribed by ANSI Std. 239-18
298-102

1. FOREWORD

One of important goals of the demining mission is a reliable differentiation between land mines and clutter, which would decrease the false alarm rate. This project can be considered as a new approach to this issue, via a new method for solutions of inverse problems. It is natural, therefore, to test such an approach on a mathematical model first in order to see its main features. While being at an Army's demonstration of a demining process at AP Hill (VA) in 1998, we observed that the process of detection and identification of land mines by a hand-held GPR can be subdivided into two subprocesses, which, using an analog with medical imaging, we call: (i) screening and (ii) diagnostics. In the screening procedure one identifies horizontal coordinates of possible mine-like targets, many of which might be clutter. The screening procedure should be very rapid. The diagnostic procedure, however, is slower. This is a procedure of differentiating between mines and clutter. Another term for this is "classification" procedure. All targets being detected on the first stage should be checked out again. Finally, all targets, being identified as possible land mines should be removed from soil by soldiers. Since the diagnostic procedure usually takes many hours, even for a small area, it would be quite helpful to develop new methods, which would speed it up very essentially, while still maintaining high reliability.

From this prospective, the goal of this project was to develop a new mathematical approach of an inverse problem, which potentially might lead to a successful diagnostic procedure for land mines. The input data for an inverse problems are measurements by a GPR of a back reflected electric signal on an array of antennas, using a frequency sweep. The output of the solution of the inverse problem is the vector consisting of coordinates of a target(s), as well as, dielectric permittivity ε and electric conductivity σ within a target(s). On the next stage, this vector is supposed to be used as an input for the classification procedure. Since we are interested in imaging of plastic antipersonnel mines with a low depth of burial ranging from 1 cm to 10 cm, we work with a high frequencies penetrating up to this depth. The range of these frequencies is from 0.5 GHz to 3 GHz.

The solution of the corresponding inverse problem, however, is quite a challenging issue in its own right. This issue was addressed in this project. Specifically, a new method for the corresponding inverse problem was developed, which is a second generation of the so-called Elliptic Systems Method (ESM), being previously developed by the Co-PIs for Diffusion Tomography with medical applications [**10, 12-14**]. (In this report references in bold face letters refer to Bibliography section. References like [1] refer to section fitted "Listing of all publications and technical reports supported under this grant.") The new method provides accurate estimates of the above parameters in about six minutes of CPU time on SGI Origin 200 with one processor. This time frame is realistic for the diagnostic purpose. It can also be decreased if using several processors. The key reason for such a small time frame is that in this new approach the resulting linear system has a differential, rather than conventional integral form. This means, in turn, that the matrices to be inverted are sparse, rather than full, the very property, which enables one to apply modern techniques of Numerical Linear Algebra for their inversion. We want to point out that almost all conventional methods of

solutions of inverse problems are relying on solutions of ill-posed integral equations, which inevitably lead to large full matrices to be inverted, thus requiring a significant CPU time.

Since methods of integral equations are quite time consuming, as compared with ours, we compare our technique with the best competing approach, being initially developed by a well known German expert in inverse problem F. Natterer six years ago [**19**]; also see follow up publications [**5,6**]. Thus, we modified our algorithm accordingly. Naturally, the modified variant is also based on resulting differential, rather than integral operators. In the view of possible applications to the experimental data an important advantage of the second version is that the differentiation of the data with respect to the frequency is not required, unlike the first version. On the other hand, while both versions have a similar performance in terms of timing and locations of targets, the first one still often provides better values of electrical parameters within targets, which is the key for the diagnostic goal. Since the development of computational tols of the project was very time consuming, we did not have sufficient time left to work on the experimental data. Our modified algorithm is an *advanced* version of Natterer's method, since we calculate the resulting matrices precisely, whereas only diagonal elements of matrices are counted in [**5,6,19**]. Thus, if using only those elements (i.e., if literally following the idea of Natterer), images by the second method would be much worse than by the first one.

Although the topic of the project is inverse problems, one must always possess a rapid algorithm for solutions of corresponding forward problems, when working with the inverse. However, when starting the work on this project, we discovered that such an algorithm simply did not exist at that time, for the high frequency range we used. Therefore, the very first, although axillary task was to develop such a method.

Thus, major tasks of this project are ones listed below. Work on each of these tasks required approximately one year.

Task 1 (axillary)

Development of an efficient numerical method for the solution of the forward GPR problem for the high frequencies.

Task 2

Development of a second generation of the ESM for the solution of the GPR inverse problem.

Task 3

Development of the modified version of the method of Task 2 and comparison.

All these three tasks were successfully completed. Summary of results in given below.

2. TABLE OF CONTENTS

4. STATEMENT OF THE PROBLEM UNDER STUDY	**5**
4.1. Partial Differential Equation	**5**
4.2. Ranges of Parameters	**5**
4.3. Statement of the Forward Problem	**6**
4.4. Statement of the Inverse Problem	**7**
5. SUMMARY OF THE MOST IMPORTANT RESULTS	**9**
5.1. Task 1 (Axillary). Development of an Efficient Numerical Method for the Solution of the Forward GPR Problem for High Frequencies	**9**
5.2. Task 2. Development of a Second Generation of the ESM for the Solution of the Inverse Problem	**10**
5.2.1. Integro-Differential Equation	**11**
5.2.2. An Idealized Case of Complete Data Collection	**13**
5.2.3. Incomplete Data Collection	**15**
5.3. Task 3. Development the Modified Version of the Method of Task 2 and Comparison	**18**
5.3.1. Description of the *H*-method	**18**
5.3.2. Brief description of Natterer's method	**19**
5.4. Numerical Experiments	**20**
5.4.1. The most practically important case of a simple target filled with TNT	**20**
5.4.2. Three targets filled with TNT	**24**
5.4.3. Conclusion for Comparison of *p* and *H* Methods	**25**
5.5. Conclusions	**25**
5.6. Possible Future Direction of Research	**27**
6. LISTING OF ALL PUBLICATIONS AND TECHNICAL REPORTS SUPPORTED BY THIS GRANT	**29**
7. LIST OF ALL PARTICIPATING SCIENTIFIC PERSONNEL	**31**
8. REPORT ON INVENTIONS	**32**
10. BIBLIOGRAPHY	**33**

3. LIST OF ILLUSTRATIONS AND TABLES

1.	Table 1.	Approximate values of $\varepsilon_r, \tan(\delta), k^2, k$ and λ for Different Soil Moistures and TNT of $f = 1GHz$	5
2	Figure 1.	Re$[h(x)]$ for a circular shaped single target filled with TNT	21
3.	Figure 2.	Re$[H(x,\omega)]$ or a function of the frequency f at $x = (10,0)$	21
4.	Figure 3.	Re$[H_{x_2}(x,\omega)]$ as a function of the frequency f at $x = (10,0)$	22
5	Figure 4.	Re$[H(x_1,\omega)]$ for $\omega_0 = 1.0 \bullet 2\pi GHz$ as a function of x_1 along $\{x_2 = 0\}$	22
6	Figure 5.	Re$\left[h_{imaged}(x)\right]$ for the solution of the inverse problem by the p method	22
7	Figure 6.	Re$\left[h_{imaged}(x)\right]$ for the solution of the inverse problem by the H method.	22
8	Figure 7.	Horizontal cross-sections of Re$\left[h_{imaged}(x)\right]$ after two sweeps using the p method for different values of $\omega_{\max}$.	23
9	Figure 8.	Horizontal cross-sections of Re$\left[h_{imaged}(x)\right]$ after one sweep using the H method for different values of $\omega_{\max}$.	23
10	Figure 9.	Vertical cross-sections of Re$\left[h_{imaged}(x)\right]$ after two sweeps using the p method for different values of $\omega_{\max}$.	24
11	Figure 10.	Vertical cross-sections of Re$\left[h_{imaged}(x)\right]$ after one sweep using the H method for different values of $\omega_{\max}$.	24
12	Figure 11.	Re$[h(x)]$ for three mine-like targets of various sizes.	25
13	Figure 12.	Final reconstruction of Re$\left[h_{imaged}(x)\right]$ after one sweep using the p method.	26
14	Figure 13.	Final reconstruction of Re$\left[h_{imaged}(x)\right]$ after one sweep using the H method.	26
15	Figure 14.	Horizontal cross-sections of Re$\left[h_{imaged}(x)\right]$ using the p and H methods.	27

4. STATEMENT OF THE PROBLEM UNDER STUDY

4.1. Partial Differential Equation

The GPR signal is modeled here as a polarized electric plane wave $E_0 = (0, 0, \exp(i\omega\sqrt{\mu\varepsilon_0} \cdot x_2)) \cdot \exp(-i\omega t)$ propagating along the positive direction of x_2-axis in the half space $\{x_2 < 0\}$. Here $\omega = 2\pi f$ is the angular frequency of the signal, $\mu = 4\pi \cdot 10^{-7}$ *Henry/m* is the magnetic permeability and $\varepsilon_0 = 8.854 \cdot 10^{-12}$ *Farad/m* is the dielectric permittivity of free space. It is assumed that $\{x_2 < 0\}$ is air and $\{x_2 > 0\}$ is ground, where mine-like targets are located. All functions below depend only on two spatial variables $(x_1, x_2) = x$. Let $E(x, \omega) = (0, 0, u(x, \omega)) \cdot \exp(-i\omega t)$ be the electric field. Then the following Helmholtz-like PDE for the function $u(x, \omega)$ can be derived from Maxwell's system [3]

$$\nabla^2 u + k^2(x, \omega)u = 0. \tag{4.1}$$

Here the function $k^2(x, \omega)$ has the form $k^2(x, \omega) = \omega^2\mu\varepsilon(x) + i\omega\mu\sigma(x)$, where $\varepsilon(x)$ and $\sigma(x)$ are respectively the dielectric permittivity and the electric conductivity of the medium, and μ is the magnetic permeability, which is assumed to be constant everywhere and equal to its value in free space, $\mu \equiv const$. We also assume that $\varepsilon = \varepsilon_0$ in air.

4.2. Ranges of Parameters

It is useful first to establish ranges of parameters in the PDE (4.1). All units below are given in SI system. The frequency of the signal $f = \dfrac{\omega}{2\pi}$ is between 0.5 GHz and 3 GHz, i.e., $f \in (0.5, 3) \cdot 10^9 \dfrac{1}{\text{sec}}$. Let $\varepsilon = \varepsilon_r\varepsilon_0$ where ε_r is the relative dielectric constant. In air $\varepsilon_r = 1$ and $\sigma = 0$. We introduce the so-called "loss tangent" as [9]

$$\tan(\delta) = \frac{\sigma}{\omega\varepsilon}. \tag{4.2}$$

Then

$$k^2 = \omega^2\mu\varepsilon[1 + i \cdot \tan(\delta)]. \tag{4.3}$$

We assume that the loss tangent does not depend on ω, i.e., $\dfrac{\partial}{\partial\omega}[\tan(\delta)] = 0$. This condition is a requirement for the presented imaging algorithm. It is satisfied with sufficient accuracy in many practical scenarios of land mine detection.

The approximate values of the parameters ε_r, $\tan(\delta), k^2, k$ and the wavelength $\lambda = 2\pi/\operatorname{Re}(k)$ for different soil moistures as well as for trinitrotoluene (TNT) are given in Table 1 for the frequency $f = 1$ GHz. In this table we use the data of [7]

Table 1. Approximte Values of $\varepsilon_r, \tan(\delta), k^2, k$ and λ for Different Soil Moistures and TNT at $f = 1$ GHz

Medium	ε_r	$\tan(\delta)$	k^2 $\left[\frac{1}{m^2}\right]$	k $\left[\frac{1}{m}\right]$	$\lambda[cm]$
Air	1	0	439.2	21	30
Dry soil	30	0.025	$1273 + i \cdot 31$	$35.7 + i \cdot 0.43$	17
Wet soil, 5% moisture	4	0.22	$1756 + i \cdot 395$	$42 + i \cdot 4.7$	15
TNT	2.86	0.0018	$1256 + i \cdot 2.26$	$35.4 + i \cdot 0.03$	17.7

4.3. Statement of the Forward Problem

We assume that the electrical parameters ε and σ have constant background values everywhere in the ground, except in the mine-like targets, whose sizes are small, as compared with the size of the region of interest. Let $k_0 = k_0(x_2, \omega)$ be the function k in (4.3) for the background medium. Then this function has a discontinuity on the air/ground interface,

$$k_0^2 = \begin{cases} \omega^2 \mu \varepsilon_0, & \text{for } x_2 < 0 \\ \omega^2 \mu \varepsilon_0 \varepsilon_r [1 + i \cdot \tan(\delta)], & \text{for } x_2 > 0. \end{cases} \tag{4.4a}$$

Let $u_0 = u_0(x_2, \omega)$ be the solution of the PDE (4.1), which corresponds to the initial plane wave without targets present. Then u_0 consists of the initial, reflected, and transmitted plane waves [9],

$$u_0 = \begin{cases} e^{ik_0 x_2 + R(k_0) e^{-ik_0 x_2}}, & \text{for } x_2 < 0 \\ T(k_0) e^{ik_0 x_2}, & \text{for } x_2 > 0, \end{cases} \tag{4.4b}$$

where $R(k_0)$ and $T(k_0)$ are the reflection and transmission coefficients given by

$$R(k_0) = \frac{k_0^- - k_0^+}{k_0^- + k_0^+}, \qquad T(k_0) = \frac{2k_0^-}{k_0^- + k_0^+}. \tag{4.4c}$$

Here k_0^- and k_0^+ are the values of k_0 for $x_2 < 0$ and $x_2 > 0$ respectively. The presence of these coefficients ensures the continuity of the function u_0 together with its first derivatives at $\{x_2 = 0\}$.

We seek a solution of the equation (4.1) in the form $u = u_0 + v$, where the function $v(x, \omega)$ represents the wave scattered by mine-like targets with compact supports in $R^2_+ = \{x_2 > 0\}$. Hence, this function satisfies the following PDE

$$\nabla^2 v + k^2 v = -g, \qquad x \in R^2, \tag{4.5}$$

where $k^2 = k_0^2$ outside of the targets and

$$g(x, \omega) = \begin{cases} 0, & \text{outside targets} \\ (k^2 - k_0^2) u_0, & \text{inside targets.} \end{cases}$$

In addition, we impose Sommerfeld radiation boundary conditions at infinity

$$\lim_{r \to \infty} \sqrt{r} \left(\frac{\partial v}{\partial r} - ik_0 v \right) = 0, \tag{4.6}$$

where $r = \sqrt{x_1^2 + x_2^2}, \mathrm{Im}(k_0) > 0$ and the limit holds uniformly in all directions. The uniqueness and existence of the solution of the problem (2.6), (2.7) was proven in [3] for the 3-D case. It follows from the proof in [3] that similar results hold in the 2-D case for functions $v \in H^{1,-s}$ with $s > 1/2$, where $H^{1,s} = \{\omega : D^a \omega \in L^{2,s}, |\alpha| \leq 1\}$ and $L^{2,s}(R^2) = \left\{v : (1 + |x_2|^2)^{s/2} v \in L_2(R^2)\right\}$. Likewise, if D is any bounded domain such that either $D \subset R^2_+$ or $D \subset R^2_-$, then $v \in H^2(D)$. It follows also from [3] that if in (4.4a)

$\tan(\delta) > 0$, then for $x_2 \geq 0$ the functions $v(x,\omega), v_{x_1}(x,\omega)$ and $v_{x_2}(x,\omega)$ decay exponentially as $\omega \to \infty$. The function $(k^2 - k_0^2)(x)$ is assumed to be bounded and to have compact support in $\{x_2 > \gamma\}$ for some positive constant γ.

It is natural to consider in practical computations a bounded domain G_L, which is obtained by a cut-off of the infinite space R^2. For the numerical solution of the *forward* problem, we consider a square $G_L = \{|x_1|, |x_2| \leq L\}$. In this case the condition (4.6) is replaced with

$$v_{x_1} \mp ik_0 v|_{x_1=\pm L} = 0, \qquad v_{x_2} \mp ik_0 v|_{x_2=\pm L} = 0. \tag{4.7}$$

So, below we will always assume that the boundary value problem (4.5), (4.7) has an unique solution $v \in H^1(G_L)$. By the well known results for elliptic equations, this implies, in turn, that $v \in H^2(G_L \cap \{x_2 > 0\})$ and $v \in H^2(G_L \cap \{x_2 < 0\})$. A natural question to ask would be about the influence of the value of the cut-off constant L on the resulting solution v. It was shown numerically in [1] that if the targets are located "well within" the square G_L (i.e., far from the boundaries), then, for the range of parameters listed in Table 1, the resulting value of the function $v(x,\omega)$ for points x located near the air/ground interface $\{x_2 = 0\}$ is independent of L as long as $L \geq 53$ cm. For this reason, for the solution of the *inverse* problem we chose a smaller rectangle $\Omega \subset G_L, \Omega \subset R^2_+$. First we generate the data $v|_{x_2=0}$ and $v_{x_2}|_{x_2=0}$ for the inverse problem using the solution of the forward problem in the domain G_L with $L = 1.5$ m. To solve the inverse problem, we use the rectangle

$$\Omega = \{x = (x_1, x_2) : |x_1| < L_1 = 0.6 \text{ m}, 0 < x_2 < L_2 = 0.4 \text{ m}\}.$$

In doing this, we use the following boundary conditions for the function v on the side and top boundaries of Ω :

$$v_{x_1} \mp ikv|_{x_1=\pm L_1} = 0 \tag{4.8a}$$

$$v_{x_2} - ikv|_{x_2=L_2} = 0. \tag{4.8b}$$

As to the boundary conditions on the bottom boundary $v|_{x_2=0}$ and $v_{x_2}|_{x_2=0}$, they are used as an input data for the inverse problem and, thus are taken from the solution of the forward problem in the domain G_L.

4.4. Statement of the Inverse Problem

Let ε_1 and $\tan(\delta_1)$ be the values of the parameters ε and $\tan(\delta)$ everywhere in the ground, except for the mine-like targets. Then

$$\varepsilon(x) = \varepsilon_1 + h_\varepsilon(x), \qquad \tan(\delta) = \tan(\delta_1) + h_\sigma(x), \tag{4.9}$$

where the perturbations $h_\varepsilon(x)$ and $h_\sigma(x)$ are due to the presence of the mine-like targets. Hence, the determination of these functions would yield both the locations of these targets and the values of the electrical parameters within them. Since the loss tangent does not depend on the frequency ω, we introduce a perturbation $h(x)$ of the background coefficient $k_0^2(x,\omega)$ as a "whole,"

$$h(x) = \frac{k^2(x,\omega) - k_0^2(x,\omega)}{k_0^2(x,\omega)}. \tag{4.10}$$

Hence,

$$k^2(x,\omega) = k_0^2[1 + h(r)] = \omega^2 k_{0s}^2[1 + h(x)], \tag{4.11}$$

where $k_{0s}^2 = k_0^2/\omega^2$. By (4.9)-(4.11) the function $h(x)$ can be obtained from the functions $h_\varepsilon(x)$ and $h_\sigma(x)$ through the following transformation:

$$h = \frac{h_\varepsilon + i[\varepsilon_1 h_\sigma + h_\varepsilon \tan(\delta_1) + h_\varepsilon h_\sigma]}{\varepsilon_1[1 + i\tan(\delta_1)]}.$$

Once the complex valued function $h(x)$ has been obtained from the solution of the inverse problem, one can recover the perturbations of the physical parameters by using the formulas:

$$h_\varepsilon = \varepsilon_1[\mathrm{Re}(h) - \tan(\delta_1) \cdot \mathrm{Im}(h)],$$
$$h_\sigma = \frac{\mathrm{Im}(h) \cdot [1 + \tan^2(\delta_1)]}{1 + \mathrm{Re}(h) - \tan(\delta_1) \cdot \mathrm{Im}(h)}.$$

Inverse Problem. *Given functions* $\varphi(x_1,\omega), \psi(x_1,w)$ *defined as*

$$\varphi(x_1,\omega) = v|_{x_2=0}, \tag{4.12a}$$

$$\psi(x_1,\omega) = v_{x_2}|_{x_2=0}, \tag{4.12b}$$

for $x_1 \in (-L_1, L_1)$, $\omega \in (\omega_{\min}, \omega_{\max})$, *determine the perturbation function* $h(x)$.

Here $(\omega_{\min}, \omega_{\max})$ is the available frequency band, over which measurements are performed. We assume that measurements are performed at points on a certain interval $(-L_1, L_1)$ of the line $\{x_2 = 0\}$ located on the air/ground interface. To explain a possible way to evaluate the normal derivative ψ in (4.12b), we observe that if the function φ is given, one can uniquely solve the boundary value problem (4.5), (4.8), (4.12a) in the air, i.e., for $\{x_2 < 0\} \cap \{|x_1| < L_1\}$, where no targets are present. This is sufficient to determine the function ψ. Another option to obtain the normal derivative v_{x_2} would be to measure not only the third component E_3 of the electric field E, but the first component H_1 of the magnetic field H as well, since Maxwell's system implies in our case $E_{3x_2} = i\omega\mu H_1$.

The resulting PDE for the function v is

$$\nabla^2 v + \omega^2 k_{0s}^2 v + \omega^2 k_{0s}^2 h(x) v = -\omega^2 k_{0s}^2 h(x) u_0, \tag{4.13}$$

where $h(x)$ is a bounded function with compact support in Ω and the function u_0 is given by (4.4b) (for $x_2 > 0$). We will assume that the medium of interest Ω is basically homogeneous, except for a few mine-like targets whose sizes are small compared to the size of Ω. This suggests the related assumption that $\|h\|_{L_2(\Omega)} \ll \|s\|_{L_2(\Omega)}$, where the function $s(x) \equiv 1$. Note that function v depends nonlinearly on the function h. However, we will consider a linearized inverse problem, assuming that perturbations are small, as compared with the background. Hence, linearization leads to dropping the $h(x)v$ term in (4.13). This approach was used previously in publications about the ESM **[10, 12-14]**. The assumption about the linearization can actually be relaxed if using Newton-like updates **[10, 12-14]**. However,

limited testing of those updates for the range of parameters we used did not show significant improvement of the images.

Thus, below we will consider the inverse problem only for the *linearized*, with respect to h, equation (4.13), while the data simulation for the forward problems will still be done for the original equation (4.13). Linearization of (4.13) with respect to h leads to

$$\nabla^2 v + \omega^2 k_{0s}^2 v = -\omega^2 k_{0s}^2 h(x) u_0 \tag{4.14}$$

5. SUMMARY OF THE MOST IMPORTANT RESULTS.

In this section we discuss only results of tasks 1-3, which are the most important ones in this project. These results were obtained by M. V. Klibanov, Yu. A. Gryazin and T. R. Lucas. It should be noted that some results of a lesser importance were also obtained by other members of the scientific personnel : T. P. Weldon, V. J. Patel [4,6] and S. Pamyatnikh. However, these results are not discussed here.

5.1. TASK 1 (AXILLARY). DEVELOPMENT OF AN EFFICIENT NUMERICAL METHOD FOR THE SOLUTION OF THE FORWARD GPR PROBLEM FOR HIGH FREQUENCIES

Since this is axillary (although an important) task, we will provide a rather brief description of this development referring to [1,3] for details.

As it was pointed out above, the very first difficulty we faced in this project was the absence of a rapid algorithm for the solution of the forward problem for small wavelengths λ we used. For example, as it follows from Table 1, for the frequencies $f \in (0.5, 3)$ GHz the

$$\lambda \in \begin{cases} (5, 35) \text{ cm, in the ground} \\ (10, 60) \text{ cm, in the air} \end{cases} \tag{5.1}$$

This range of wavelengths significantly affects the grid size in the Finite Differences Solution for both the forward and the inverse problem. In order to calculate the forward problem accurately, one should use at least 10 grid points per wavelength. Suppose, for example that one wants to calculate the function u in a square region of 2 m $\times$ 2 m. Then, because of (5.1), this would mean that one should use at least 400 $\times$ 400 grid for $\lambda = 5$ cm. When analyzing this problem, we quickly realized that standard direct solve routines, such as LAPACK, for example, are inapplicable here, since they provide data generation for the inverse problem in about 6 hours of CPU time on Silicon Graphics Origin 200 (SGI). This was a strong motivation for us to develop a new efficient algorithm for the forward problem.

The idea is to develop a high quality Krylov subspace based method (GMRES). First, we approximate the differential operator of the Helmholtz equation (4.5) in the square G_L with finite differences assuming the coefficient k_0^2 depends only x_2. In the resulting matrix operator we replace the Sommerfeld-like boundary condition (4.8) with either Dirichlet or Neumann boundary condition. The resulting matrix is then used as a pre-conditioner to

accelerate the convergence of GMRES. To invert this matrix effectively, eigenvectors of the corresponding operator are found and used as an orthonormal basis. Such an orthonormal basis is possible to find, because both Dirichlet and Neumann boundary conditions generate self adjoint matrices, which is the key reason of replacement of Sommerfeld boundary conditions with either of the above two in this pre-conditioner. This leads to a diagonal matrix to invert, which obviously can be done very rapidly. Iterations are used "with respect" to both boundary conditions (in order to get boundary conditions (4.8) in the end), and the mine-like targets. In order to generate data on many frequencies, a high order extrapolation technique is used to give a starting value for a higher frequency given values at the lower ones. This, in combination with the pre-conditioner, leads to a total CPU time of about 5 minutes for 150 frequencies on a 199×199 grid.

The idea of the pre-conditioner was published in [3]; and complete details were published in [1]. It is worthwhile to mention here that this work received a warm reception from the Editorial Board of Journal of Computational Physics [1], and one of figures of [1] was selected for the cover of the issue.

In all numerical examples below data simulation for the inverse problems were provided by solution of the forward problem (4.5), (4.8) using the method of [1]. In particular, some results of solutions of this problem by this method are presented on Figs. 2-4.

5.2 TASK 2. DEVELOPMENT OF A SECOND GENERATION OF THE ESM FOR THE SOLUTION OF THE INVERSE PROBLEM

We refer to this algorithm as the "p-method" because we compare it below with an analog of Natterer's method, which we call "H-method". Results of this section are published in [12].

As it is always the case in the field of inverse problems, it is useful to establish an uniqueness result first. This result is formulated in Theorem 5.1.

Theorem 5.1. *For $x_2 > 0$ let $k_0^2 = \omega^2 k_{0s}^2$, where the complex constant k_{0s} was defined in (4.11), does not depend on ω and x, $\mathrm{Re}(k_{0s}) > 0$ and $\mathrm{Im}(k_{0s}) > 0$. Suppose the functions $\varphi(x_1, w)$ and $\psi(x_1, \omega)$ in (4.12a,b) are given for $x_1 \in (-\infty, \infty)$ and $\omega \in (\omega_{\min}, \omega_{\max})$, where $0 < \omega_{\min} < \omega_{\max}$. Then there exists at most one pair of functions (v, h) satisfying (4.6), (4.12), (4.14) in R^2_+ such that $h(x)$ is a bounded function with compact support in $\{x_2 > \gamma\}$ with a positive constant γ, and $v \in H^{1,-s}(R^2_+)$ with $s > 1/2$.*

An obvious inconvenience of the equation (4.14) is that this is one equation with two unknown functions $h(x)$ and $v(x, \omega)$ in it. The **key** idea of the ESM is to eliminate the unknown perturbation term $h(x)$ from (4.14) using differentiation with respect to a "free" parameter ω. This leads to an integro-differential equation, in which integrals are taken with respect to ω (see below), supplied by the boundary condition resulting from (4.8), (4.12). Naturally, the next question is: *How to solve the resulting boundary value problem (BVP)?*

In the first generation of this ESM, which was aimed on medical applications and was applied to the time dependent diffusion equations, integrals were eliminated via truncated generalized Fourier series with respect to time [**10-14**]. As a result, a BVP for an elliptic

system was obtained (the latter led to the name of this method). A shortcoming of this specific implementation was that while locations of abnormalities were imaged very accurately, values of unknown coefficients within them were estimated with a poor accuracy. This is clearly unacceptable for the applications to imaging of land mines, in which an important input in the process of differentiation of land mines from clutter would come from the values of electrical parameters within those targets. This motivated the development of the second generation of the ESM, in which the BVP for the integro-differential equation is solved directly, i.e., without elimination of integrals. The resulting algorithm provides accurate images of both locations of targets and values of electrical parameters within them.

5.2.1. INTEGRO-DIFFERENTIAL EQUATION

Note that because of (4.4), the function u_0 in (4.14) has the form

$$u_0 = T(k_0)\exp(i\omega k_{0s} x_2). \tag{5.1}$$

The function $h(x)$ in (4.14) can be isolated by dividing both sides by $\omega^2 k_{0s}^2 u_0$. Let

$$H(x,\omega) = \frac{v}{\omega^2 k_{0s}^2 u_0}. \tag{5.2}$$

Then because of (5.2), (4.14) becomes

$$\nabla^2 H + 2i\omega k_{0s} H_{x_2} = -h(x), \quad x \in \Omega \tag{5.3}$$

with the corresponding boundary conditions

$$H|_{x_2=0} = \tilde{\varphi}(x_1,\omega), \qquad H_{x_2}|_{x_2=0} = \tilde{\varphi}(x_1,\omega), \qquad \omega \in (\omega_{\min},\omega_{\max}), \tag{5.4a}$$

$$H_{x_1} \pm i\omega k_{0s} H|_{x_1=\pm L_1} = 0 \tag{5.4b}$$

$$H|_{x_2=L_2} = 0,$$

where functions $\tilde{\varphi}$ and $\tilde{\psi}$ are obtained from the functions φ and ψ of (4.12) in an obvious way.

To eliminate the function $h(x)$ from (5.3), differentiate this equation with respect to ω. Let

$$p(x,\omega) = \frac{\partial H}{\partial \omega}.$$

We assume that for every $x \in \Omega$

$$\lim_{\omega\to\infty} H(x,\omega) = 0 \tag{5.5}$$

and

$$p, p_{x_2} \in L_1(\omega_{\min},\infty), \tag{5.6}$$

as functions of ω. In the case when the 2-D boundary value problem (4.5), (4.6) is considered over the whole space R^2, including the case of the linearized (with respect to $h(x)$) equation (4.14), conditions (5.5) and (5.6) easily follow from the above mentioned result of [3]. However, at this point, we have not been able to rigorously establish these conditions for the case of the finite domain Ω. Still, we have observed them in the computations of solutions of the forward problem. We assume below that conditions (5.5) and (5.6) hold. Hence,

$$H(x,\omega) = -\int\limits_{\omega}^{\infty} p(x,\tau)d\tau.$$

However, we will use approximation

$$\int\limits_{\omega}^{\infty} p(x,\tau)d\tau \approx \int\limits_{\omega}^{\omega_{\max}} p(x,\tau)d\tau$$

and thus

$$H(x,\omega) = -\int\limits_{\omega}^{\omega_{\max}} p(x,\tau)d\tau. \tag{5.7}$$

In (5.7) "$\approx$" is replaced with "$=$" for the sake of notational convenience.

Let $g_1(x_1,\omega) = \frac{\partial}{\partial\omega}\tilde{\varphi}(x_1,\omega)$ and $g_2(x_1,\omega) = \frac{\partial}{\partial\omega}\tilde{\psi}(x_1,\omega)$. Then because of (5.3), (5.4) and (5.7), we obtain

$$\nabla^2 p + 2i\omega k_{0s} p_{x_2} = 2ik_{0s}\int\limits_{\omega}^{\omega_{\max}} p_{x_2}(x,\tau)d\tau, \quad x \in \Omega, \tag{5.8a}$$

$$p|_{x_2=0} = g_1(x_1,\omega), \qquad p_{x_2}|_{x_2=0} = g_2(x_1,\omega), \tag{5.8b}$$

$$p_{x_1} \mp i\omega k_{0s} p|_{x_1=\pm L_2} = \mp ik_{0s}\int\limits_{\omega}^{\omega_{\max}} p(x,\tau)d\tau|_{x_1=\pm L_1}, \tag{5.8c}$$

$$p_{x_2}|_{x_2=L_2} = 0. \tag{5.8d}$$

Thus, we have obtained the boundary value problem (5.8) for the integro-differential equation (5.8a) with Volterra-like integrals being present in both the equation itself and the boundary conditions. Once the function p is found from (5.8), the function $h(x)$ can be easily recovered by backwards calculations: First, the function $H(x,\omega)$ is available through (5.7); next, the function $h(x)$ can be calculated from (5.3) evaluated at $\omega = \omega_{\min}$. Therefore, the principal computational question becomes: *How to solve the boundary value problem (5.8)*? This question is addressed below.

The problem (5.8) is overdetermined, because both Dirichlet and Neumann boundary conditions are given at $x_2 = 0$ in (5.6). There is no guarantee that the solution of the overdetermined problem (5.8) exists. Therefore, the idea is to find such a function p, which

satisfies conditions (5.8) in an *optimal* sense. That is, we want to find a minimal norm solution. In terms of matrix equations resulting from the finite difference approximation of (5.8) for each value of ω, this means that we will find a *normal* solution of the matrix system for each ω, which is a parameter of this system.

5.2.2. AN IDEALIZED CASE OF COMPLETE DATA COLLECTION

To explain our idea better, we assume in this subsection that both Dirichlet and Neumann boundary conditions are given over the entire boundary $\partial\Omega$. Then (5.8) becomes

$$A^{\omega}(p) := \nabla^2 p + 2i\omega k_{0s} p_{x_2} = 2ik_{0s} \int_{\omega}^{\omega_{\max}} p_{x_2}(x,\tau)d\tau, \qquad x \in \Omega, \tag{5.9a}$$

$$p|_{\partial\Omega} = \tilde{g}_1(x,\omega), \qquad \frac{\partial p}{\partial \nu}|_{\partial\Omega} = \tilde{g}_2(x,\omega), \tag{5.9b}$$

where A^{ω} is the differential operator in the left hand side of (5.8a), and the functions $\tilde{g}_1$ and $\tilde{g}_2$ are given for $(x,\omega) \in \partial\Omega \times (\omega_{\min}, \omega_{\max})$, with $\tilde{g}_1|_{x_2=0} = g_1, \tilde{g}_2|_{x_2=0} = g_2$. First, consider the more general problem

$$A^{\omega}(P) = S(x,\omega), \tag{5.10a}$$

$$P|_{\partial\Omega} = \tilde{g}_1, \qquad \frac{\partial p}{\partial \nu}|_{\partial\Omega} = \tilde{g}_2, \tag{5.10b}$$

where the function $S \in L_2(\Omega \times (\omega_{\min}, \omega_{\max}))$.

Important Remark. We note that if the right hand sides of equations (5.3), (5.4) are zeros, then $H \equiv 0$. Similar statement is true for the system (5.8): if the right hand sides of equations (5.8) equal zero, then $p \equiv 0$. This follows from the well known theorem about uniqueness of solution of the so-called "Cauchy problem" for the elliptic equation, cf. **[15, 16]**. This observation is important for our computations, because it justifies linear independence of column of matrices A_d^n and $B(\beta_j)$ below, provided that the grid size is sufficiently small. This, in turn, implies that matrices $A_d^{n*}A_d^n$ and $B^*(\beta_j)B(\beta_j)$ are Hermitian Positive Definite ones, which enabled us to use Conjugate Gradient Method for their solution.

We seek solution of the problem (5.10) in the minimal norm sense as

$$\|A^{\omega}(P) - S(x,\omega)\|_{L_2(\Omega)} \to \min, \text{ for every } \omega \in (\omega_{\min}, \omega_{\max}), \tag{5.11a}$$

$$P|_{\partial\Omega} = \tilde{g}_1, \qquad \frac{\partial P}{\partial \nu}|_{\partial\Omega} = \tilde{g}_2, \tag{5.11b}$$

$$P(x,\omega) \in H^2(\Omega) \text{ for each fixed } \omega \in [\omega_{\min}, \omega_{\max}] \text{ and } \sup_{\omega \in [\omega_{\min}, \omega_{\max}]} ||P||_{H2(\Omega)} < \infty \tag{5.11c}$$

This minimization problem is equivalent to the solution of the 4th order elliptic PDE:

$$\left(A^{\omega *}A^{\omega}\right)(P) = A^{\omega *}(S), \tag{5.12}$$

plus the conditions (5.11b). Next, we replace in (5.12) the function S with the right hand side of (5.9a). Thus, we finally come up with the following boundary value problem for an elliptic integro-differential equation of the 4th order

$$\left(A^{\omega *}A^{\omega}\right)(P) = A^{\omega *}\left(2ik_{0s}\int\limits_{\omega}^{\omega_{\max}} P_{x_2}(x,\tau)d\tau\right), \qquad x \in \Omega, \tag{5.13a}$$

$$P|_{\partial\Omega} = \tilde{g}_1(x,\alpha), \qquad \frac{\partial P}{\partial \nu}|_{\partial\Omega} = \tilde{g}_2(x,\alpha), \tag{5.13b}$$

$$\text{plus the condition (5.11c)} \tag{5.13c}$$

The problem (5.13) can be solved iteratively as

$$\left(A^{\omega *}A^{\omega}\right)(P_n) = A^{\omega *}\left[2ik_{0s}\int\limits_{\omega}^{\omega_{\max}} \left(P_{n-1}\right)_{x_2}(x,\tau)d\tau\right] \tag{5.14a}$$

$$P_0 := 0 \tag{5.14b}$$

$$P_n|_{\partial\Omega} = \tilde{g}_1(x,\omega), \qquad \frac{\partial P_n}{\partial \nu}|_{\partial\Omega} = \tilde{g}_2(x,\omega). \tag{5.14c}$$

Therefore, on each iterative step n one should solve the boundary value problem (5.14) for the 4th order elliptic operator $B_\omega = A^{\omega *}A^{\omega}$ for each value of the parameter $\omega \in [\omega_{\min}, \omega_{\max}]$.

To formulate convergence result for this iterative process, we first introduce the Banach spaces $\mathcal{L}_1 = \mathcal{L}\left(C_0^{4+\beta}(\overline{\Omega}), C^{\beta}(\overline{\Omega})\right)$ and $\mathcal{L}_2 = \mathcal{L}\left(C^{\beta}(\overline{\Omega}), C_0^{4+\beta}(\overline{\Omega})\right)$ of bounded linear operators. Let $B_\omega = A^{\omega *}A^{\omega}$. Obviously, $B_\omega \in \mathcal{L}_1$. The existence of the operator $B_\omega^{-1} \in \mathcal{L}_2$ for every $\omega \in [\omega_{\min}, \omega_{\max}]$ follows from Theorem 4.1 of **[11]**. Furthermore, the perturbation theory for linear operators implies that $\sup\limits_{\omega\in[\omega_{\min},\omega_{\max}]} ||B_\omega^{-1}|| \leq M$, with a positive constant M, cf. Theorem 2.23 in Chapter 4 of **[15]**. We also assume that there exists a function $F(x,\omega)$ such that

1. $F(x,\omega) \in C^{4+\beta}(\overline{\Omega})$ for every $\omega \in [\omega_{\min}, \omega_{\max}]$, and the norms $||F(x,\omega)||_{4+\beta}$ are uniformly bounded for all $\omega \in [\omega_{\min}, \omega_{\max}]$. Here $\beta = const. \in (0,1)$.

2. $F|_{\lambda\Omega} = \tilde{g}_1(x,\omega)$ and $\frac{\partial F}{\partial \nu}|_{\partial\Omega} = \tilde{g}_2(x,\omega)$.

A method of construction of such a function F was described in **[13]**. The following Theorem can be proven using the above result concerning the operator B_ω^{-1} as well as the conventional approach to Volterra-like integral equations:

Theorem 5.2. *Let $\Omega \subset R^2$ be a convex bounded domain with $\partial\Omega \in C^\infty$. Also, assume the existence of the function $F(x,\omega)$ with the above properties. Further, let the operators A^ω have the form (5.9a) and $B_\omega = A^{\omega *}A^{\omega}$. Then for every $\omega \in [\omega_0, \omega_1]$ there exists an inverse operator $B_\omega^{-1} \in L_2$ and $\sup\limits_{\omega\in[\omega_{\min},\omega_{\max}]} ||B_\omega^{-1}||M$, where M is a positive constant; the*

boundary value problem(5.13) has an unique solution P_* *such that* $P_* \in C_0^{4+\beta}(\overline{\Omega})$ *for every* $\omega \in [\omega_0, \omega_1]$; *the iterative procedure (5.14) converges to this solution; and*

$$\sup_{\omega \in [\omega_{\min}, \omega_{\max}]} ||P_* - P_n||_{4+\beta} \leq \frac{1}{n!} K^n \left(\omega_{\max} - \omega_{\min}\right)^n,$$

where the positive constant K *depends only on the domain* Ω, *the constant* k_{0s} *in (5.9a) and the numbers* $\omega_{\min}, \omega_{\max}$.

5.2.3. INCOMPLETE DATA COLLECTION

Briefly, the idea here is as follows. Let $\omega_{\min} = \beta_0 < \beta_1 < \ldots < \beta_N = \omega_{\max}$ be a discretization of the frequency band $[\omega_{\min}, \omega_{\max}]$ with a uniform step $\triangle\omega$. Let $A_d^n := A_d^{\beta_n}$ be matrix representing the finite difference analog of the operator $\nabla^2 + 2i\omega k_{0s} \frac{\partial}{\partial x_2}$ in (5.8a), as well as, the left hand sides of boundary conditions (5.8 b-d). Let $\overline{p}^n$ be the corresponding discrete approximation of the function $P(x, \omega)$ at $\omega = \beta_n$, and $\overline{p} = (p^0, \cdots p^N)$. Further, let $S^n(\overline{p})$ be the matrix representing the finite difference approximation of the right hand sides of (5.8 a-d), in which integrals are taken from $\omega = \beta_n$ to $\omega_{\max}$ in a discrete form. Then the discrete analog of the system (5.8) is the following matrix system

$$A_d^n(\overline{p}^n) = S_d^n(\overline{p}) \tag{5.15}$$

We assume that values $\overline{p}^k$ for $k = n+1, \cdots, N$ are given and $\overline{p}^N = 0$. The system (5.15) is overdetermined, because of two boundary conditions (5.8b), rather than one. This means that the number of rows in the matrix A_d^n exceeds the number of columns. Thus, we seek a normal solution of this system as

$$\left(A_d^{n*} A_d^n\right)(\overline{p}^n) = A_d^{n*} S_d^n(\overline{p})$$

This was a brief description of our idea for the case of incomplete data collection. Details are given below in this section.

Consider the second order central finite-difference approximation of the boundary-value problem (5.8) with an uniform mesh cell size of $h_{x_1} \times h_{x_2}$, where $h_{x_1} = \frac{2L_1}{M_{x_1}}, h_{x_2} = \frac{L_2}{M_{x_2}}$ and M_{x_1} and M_{x_2} are the number of grid points in the x_1 and x_2 directions, respectively. The gridded region uses x_1 values over the interval $[-L_1 + h_{x_1}/2, L_1 - h_{x_1}/2]$ and x_2 values over $[h_{x_2}/2, L_2 - h_{x_2}/2]$. The boundary conditions (4.8b)-(4.8d) are imposed by use of a second order approximation formula centered on each boundary, using fictitious values outside of Ω, which are eliminated in setting up the matrix system. In this case the discretized system (5.0) can be written in the following form

$$\overline{A}^{\omega} \overline{p} = 2ik_{0s} h_{x_2}^2 D^1 \int_{\omega}^{\omega_{\max}} \Lambda_{x_2} \overline{p}(\tau) d\tau + \frac{4ik_s}{(2 - i\omega k_s h_{x_1})^2 h_{x_1}} D^2 \int_{\omega}^{\omega_{\max}} \overline{p}(\tau) d\tau + G, \tag{5.16}$$

where Λ_{x_2} is the central second order approximation of the first derivative in the x_2 direction;

$$D^1 = diag\left(d^1_{11}, d^1_{21}, \ldots, d_{ij}, \ldots, d^1_{M_{x_1} M_{x_2}}\right),$$

$$\text{where } \begin{cases} d^1_{11} = 0, i = 1, \ldots, M_{x_1} \\ d_{ij} = 1, i = 1, \ldots, M_{x_1}, j = 2, \ldots, i = 1, \ldots, M_{x_2} \end{cases};$$

$$D^2 = diag\left(d^2_{11}, d^2_{21}, \ldots, d^2_{ij}, \ldots, d^2_{M_{x_1} M_{x_2}}\right),$$

$$\text{where } \begin{cases} d^2_{ij} = 1, i = 1, \ldots, M_{x_1}, j = 2, \ldots, M_{x_2} \\ d^2_{ij} = 0, \text{ otherwise} \end{cases};$$

$\overline{g}^1 = \left(\overline{g}^1_1, \ldots, \overline{g}^1_{M_{x_1}}\right)^T$ and $\overline{g}^2 = \left(\overline{g}^2_1, \ldots, \overline{g}^2_{M_{x_1}}\right)^T$ are approximations of the boundary conditions (5.8b) and $G = (G_{11}, \ldots, G_{M_{x_1} 1}, G_{12}, \ldots, G_{M_{x_1} 2}, 0 \ldots, 0)^T$, where $G_{i1} = \overline{g}^1_i = \frac{h_{x_2}}{2}\overline{g}^2_1, G_{i2} = (i\alpha s h_{x_2} - 1) 2 g^1_i$.

In (5.16), $\overline{A}^\omega$ is the rectangular matrix, which consists of the finite difference approximations of the left hand sides of equalities (5.8a-d), multiplied by $h^2_{x_2}$. The number of rows in the matrix $\overline{A}^\omega$ exceeds the number of columns, because of the overdetermination in (5.8b). To find the standard least squares solution of the overdetermined system (5.16), we use the method of normal equations as in equation (5.18) below. In practice the final normal system is similar to the system, which would result from setting up the 4th order finite difference operator as in (5.13a). However the advantage of our treatment of the incomplete data case is that no explicit treatment of an unknown second boundary condition along parts of the boundary, other than $\{x_2 = 0\}$, is required. In particular no spatial weight function needs to be introduced, as it was the case in earlier works **[13,15,16]**

In principle, the system (5.16) can be solved by iterations, similar to (5.14). But because it is Volterra-like integro-differential equation, a more natural way is to use the marching method **[4]**, which produces the solution in one step. First we approximate the integral terms in the right hand side of (5.16) by a simple trapezoidal rule. For this purpose we use a regular mesh in the ω-direction:

$$\beta_u = \omega_{\min} + n \cdot \triangle\omega, \qquad \text{where } n = 0, \ldots, N \text{ and } \triangle\omega = \frac{\omega_{\max} - \omega_{\min}}{N}.$$

Then (5.16) can be rewritten in the following form

$$\overline{A}^{\beta n}\overline{p}^n = 2ik_s h^2_{x_2} D^1 \sum_{i=n}^{N-1} \Lambda_{x_2} \frac{\overline{p}^i + \overline{p}^{i+1}}{2} \cdot \triangle\omega + \frac{4ik_s}{(2 - i\beta_n k_s h_{x_1})^2} \frac{h^2_{x_2}}{h_{x_1}} D^2 \sum_{i=n}^{N-1} \frac{\overline{p}^i + \overline{p}^{i+1}}{2} \triangle\omega + G^n.$$

Finally, we obtain the system

$$A^n_d \overline{p}^n = S^n_d(\overline{p}^{n+1}, \ldots, \overline{p}^{n-1}, \overline{g}^{1,n}, \overline{g}^{2,n}), \tag{5.17}$$

where

$$A_d^n = \overline{A}^{\beta n} - ik_s h_{x_2}^2 \triangle \omega D^1 \Lambda_{x_2} - \frac{2ik_s}{(2-\beta_n k_s h_{x_1})^2} \frac{h_{x_2}^2}{h_{x_1}} \triangle \omega D^2$$

and

$$S_d^n = 2ish_{x_2}^2 \triangle \omega D^1 \sum_{i=n+1}^{N-1} \wedge_{x_2} \overline{p}^i + \frac{4ik_s}{(2-i\beta_n k_s h_{x_1})^2} \frac{h_{x_2}^2}{h_{x_1}} \triangle \omega D^2 \sum_{i=n+1}^{N-1} \overline{p}^i + G^n,$$

taking into account the assumption that $\overline{p}^N = 0$. Note that the matrix A_d^n depends only on the frequency β_n, but not on the right hand side, or the solution $\overline{p}^j$ for any value of j.

Similarly to (5.16), (5.17) is an overdetermined system. To solve it for each β_u starting from $n = N-1$ to $n = 1$, we use the normal equations method. Thus [ ], we replace (5.17) with the normal equations form

$$A_d^{n*} A_d^n(\overline{p}^n) = A_d^{n*} S_d^n(\overline{p}), \qquad n = N-1, \ldots, 1. \tag{5.18}$$

Thus, on each step n of the marching method we must solve the system (5.18).

Iterations with Respect to $H(x, \omega_{\max})$

The above described procedure relies on the formula (5.7), which is an approximation for

$$H(x,\omega) = -\int_{\omega}^{\omega_{\max}} p(x,\tau)d\tau + H(x,\omega_{\max}). \tag{5.19}$$

So, the use of (5.7) implies that the term $H(x, \omega_{\max})$ in (5.19) is neglected. In our numerical experiments, we first tested the case where this term was included. Namely, we used an accurate value for $H(x, \omega_{\max})$, which was computed by the solution of the above forward problem of data simulation. In such a case the above described inverse algorithm led to images, which were almost identical to the correct ones. Therefore, we decided to mitigate the influence of the cut-off of the function $H(x, \omega_{\max})$ by the following iterative procedure.

Step 1. We use formula (5.7), i.e., we assign $H(x, \omega_{\max}) := 0$ and compute the function $P_1(x,\omega) := P(x,\omega)$ for $\omega \in [\omega_{\min}, \omega_{\max}]$ by the procedure described above. Given $P_1(x,\alpha)$, we compute $\tilde{H}_1(x,\alpha)$ as

$$\tilde{H}_1(x,\omega) := -\int_{\omega}^{\omega_{\max}} P_1(x,\tau)d\tau, \qquad \omega \in [\omega_{\min}, \omega_{\max}]$$

Next, given the function $\tilde{H}_1(x,\omega)$, we compute the perturbation term $h_1(x)$ using $\tilde{H}_1(x,\omega)$ for the lowest value of $\omega := \omega_{\min}$, that is by (5.3)

$$h_1(x) = -\left[\nabla^2 \tilde{H}_1 + 2i\omega k_s \tilde{H}_{1x_2}\right] |_{\omega=\omega_{\min}} \tag{5.20}$$

Finally, given the function $h_1(x)$ from (5.20), we solve the forward problem (4.5), (4.7) for the function $v(x, \omega_{\max})$. Having the resulting function $v_1 := v$, we compute the function $H_1(x, \omega_{\max})$ by the formula (5.2).

Step $n > 1$. In the above procedure for the solution of the inverse problem, we modify (5.7) as

$$H_k(x, \omega) = -\int_{\omega}^{\omega_{\max}} p_k(x, \tau) d\tau + H_{k-1}(x, \omega_{\max}).$$

Then we proceed as in step 1.

We found in our numerical experiments that this iterative procedure often enables one to improve the quality of the initial image of $h(x) := h_1(x)$.

Another important problem to address here is a choice of a fast numerical method for the solution of the system (5.18). This system must be solved for many frequencies involved. In addition because of high frequencies involved, we need to use a fine spatial grid, which is similar to the above discussed case of the forward problem. Thus, if conventional Gaussian elimination techniques were used, this would be a time consuming procedure.

The first key issue to resolve here is the band limited structure of the matrix $C_d^n = A_d^{n*} A_d^n$, since it is generated by a differential operator (rather than an integral operator in a conventional setting of inverse problems). The second key issue is the fact that the columns of A_d^n are linearly independent, because of the Important Remark above. Hence the matrix C_d^n is Hermitian Positive Definite. Thus, we have chosen a preconditioned Conjugate Gradient Method using the method of nested dissection [8], but only for a small number of frequencies. In this approach we have developed an automatic algorithm for the near optional choice of frequencies ranges, over which we use the same preconditioner. This method has enabled us to dramatically reduce the overall computational time. For a discretization of 200×70, using 132 frequencies in the marching method, this approach yields a solution of less than 3 minutes for each iteration of $H(x, \omega_{\max})$ (usually two such iterations are used) using one processor on a SGI Origin 200. If using fast dual procesing techniques, this timing can be decreased by a factor of five. But even the above timing is quite acceptable for the above diagnostic procedure of land mines. More details about this method can be found in [2]. Algebraic system of section 5.5 is also solved by this method.

5.3. TASK 3. DEVELOPMENT OF THE MODIFIED VERSION OF THE METHOD OF TASK 2 AND COMPARISON

5.3.1. Description of the H-method

The H-method is a second version of the above algorithm. Unlike the first version, we do not use the differentiation of the data with respect to the frequency ω here. This seems to be more suitable in the view of possible work with the experimental data. In addition, unlike the p-method, the H-method does not use an assumption that the loss tangent is independent on frequency. Another interesting feature of the H- method is that it is a

version of Natterer's method, which is the best competing technique in the field [**5,6,19**]. This enabled us to make a comparison with the best method in the field.

Let $\overline{h}$ be the grid function approximating $h(x)$ and $B(\omega)$ be the finite difference based matrix representing the left hand sides of equations (5.3), (5.4) as a function of ω. It is important to note that $B(\omega)$ depends only on ω, k_{0s} and the spatial grid. Also, let $S^H(\omega, \overline{h}, \tilde{\varphi}, \tilde{\psi})$ be the finite difference operator for the right hand sides of (5.3), (5.4). S^H depends not only on ω, k_{0s} and the spatial grid, but also on a grid function $\overline{h}$ and, of course on the overdetermined boundary data $\tilde{\varphi}$ and $\tilde{\psi}$ evaluated at the interface grid points. Then on step j we solve the overdetermined linear system

$$B(\beta_j)\overline{H}^j = S^H(\beta_j, \overline{h}, \tilde{\varphi}, \tilde{\psi}), \tag{5.21}$$

where the vector $\overline{H}^j$ represents the finite difference approximation to the grid values of $H(x, \beta_j)$, given $\overline{h}$. Note that the system (5.3), (5.4)) gives one equation for each spatial grid point, plus one additional equation for each grid point along the air-soil interface $x_2 = 0$.

To solve the system (5.21), we use method of normal solutions, thus coming up with the system

$$B^*(\beta_j)B(\beta_j)\widehat{H}^j = B^*(\beta_j)S^H(\beta_j; \overline{h}, \tilde{\varphi}, \tilde{\psi}), \tag{5.22}$$

The system (5.22) is solved by the same method of the above system (5.18). Note that $\widehat{H}^j \neq \overline{H}^j$, i.e., systems (5.21) and (5.22) are not equivalent. Next, we use (5.1) to update $\overline{h}$ as

$$\overline{h} := -(\nabla^2 \widehat{H}^j + 2i\omega k_{0s}\widehat{H}_{x_2})|_{\omega=\beta_j} \tag{5.23}$$

where the differential operators are understood in terms of finite difference.

The complete algorithm of the H-method can now be stated as follows: Initialize $\overline{h}$ to be the zero vector. Then complete a series of sweeps (beginning each new sweep with the latest value of $\overline{h}$ from the previous sweep) as follows until the stopping criteria is satisfied.

For $j = 1 \ldots n$:

I. Solve the system (5.22) using the latest value of $\overline{h}$.

II. Use (5.23) to compute the updated value for $\overline{h}$.

III. Repeat **I-III** $k \geq 1$ times.

5.3.2. Brief description of Natterer's method

In 1995 F. Natterer and F. Wuebbeling [**19**] proposed a new elegant method for solutions of inverse problems of ultrasound imaging. This method is also based on resulting differential, rather than conventional integral operators. Later this idea was extended on other applications, by O. Dorn, et.al. [**5,6**].

Briefly, the idea of the method [**19**] is as follows. First, the solution of an overdetermined BVP (similar to one of (5.3), (5.4)) is calculated for one value of a "free" parameter under an assumption that the perturbation term (like $h(x)$) is known. This free parameter is the source position in the above referenced works, and is frequency ω in our case. That overdetermined problem is solved by the method of normal solutions, which is similar to

the above. Given the normal solution of this BVP, the value of the perturbation term is updated as the right hand side of an equation, which is similar to (5.3). Next, this updated perturbation term is used as an input for the same procedure being repeated for the next value of the free parameter. Thus, iterations are performed with respect to the value of the free parameter. It was shown numerically in **[5,6,19]** that this process often converges, if the unknown perturbation term $h(x)$ is sufficiently small.

This process was naturally called in **[19]** "propagation - backpropagation method". Indeed first, one "propagates" a "pseudo" field into the medium by solving the overdetermined BVP for an assumed value of $h(x)$. Next, one "propagates if backwards" by updating $h(x)$.

The key advantage of the algorithm **[19]** over conventional techniques is that it solves differential, rather than integral equations on each step, which is similar to the idea of the ESM. The major disadvantage of the *specific implementation* of this method in **[5,6,19]**, however, is that instead of using the entire resulting matrix for inversion, only diagonal elements of this matrix are counted in these publications. This would mean, that in the above case of H-method, only diagonal elements of the matrix $A_d^{n*}A_d^n$ in (5.18) would be counted, which would dramatically decrease the quality of the images. Thus, in order to have a fare comparison, we decided to use an advanced version of the method **[19]** by counting the entire resulting matrix, rather than its part. Although we are not making a direct comparison, but the improvement seems clear.

5.4. NUMERICAL EXPERIMENTS

The main goal of the numerical experiments presented in this section is to demonstrate and compare the properties and performances of both p and H methods for realistic ranges of parameters and frequencies. The values of the coefficients in the Helmholtz equation, which correspond to the electromagnetic properties of air, soil and different targets were presented in Table I. In the numerical experiments the background medium is a wet soil with a 5% moisture content. The targets are assumed to be filled with TNT.

The physical domain for the inverse problem is selected to be $[-L_{x_1}, L_{x_2}] \times [0, L_{x_2}]$ where $L_{x_1} = 60\ cm$ and $L_{x_2} = 40\ cm$, with a 201×71 grid. In both approaches the system was non-dimensionalized in space and frequency. However for simplicity the results are presented here in the original coordinate systems. The spatial grids selected are uniform, but do not necessarily have the same spacings in x_1 and x_2.

5.4.1. The most practically important case of a simple target filled with TNT.

First we consider a case of a simple mine-like inclusion, which seems to be the most important one for applications to diagnostics of mine-like targets. This is a circular target filled with TNT, with the center at $x = (x_1, x_2) = (10, 5)\ cm$ and a diameter of 5 cm. Thus $h(x) = (k^2_{TNT} - k^2_{wetsoil})/k^2_{wetsoil} = -0.319 - 0.152i$. The real part of the corresponding function $h(x)$ is displayed in Figure 1.

For this application simulations of the solution of the forward problem are made using the forward solution for the discrete frequencies $\omega_j \in 2\pi \cdot [0.5, 3]\ GHz$ with the step size

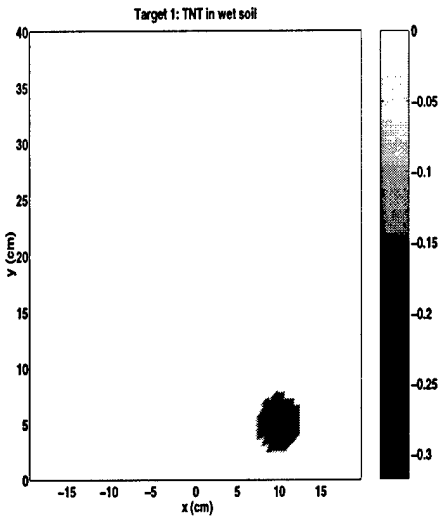

Figure 1: Re$[h(x)]$ for a circular shaped signle target filled with TNT

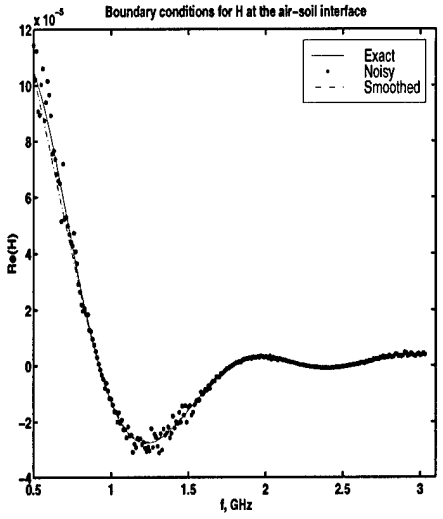

Figure 2: Re$[H(x,\omega)]$ as a function of the frequency f at $x = (10, 0)$.

of $2\pi \cdot 0.01\ GHz$. The physical domain is taken to be a square with 300 cm sides centered about the air-soil interface, and a 400×400 point computational grid is used to achieve accuracy at the higher frequency values. Two of the studies to be made here consider the effect of various choices of $\omega_{\min}, \omega_{\max}$ and the frequency spacing $\Delta\omega$ on the quality of the inverse problem solution.

For Figures 2, 3 and 4 the solid line represents the real parts of the original values obtained through the solution of the forward problem, the stars, which are the data originally received by the algorithm, represent those values with $\sigma = 0.1$ multiplicative Gaussian noise added, and the dot-dash line the result after a C^2 cubic spline smoothing process [1]. Figures 2 and 3 display the real parts of $H(x,\omega) = \tilde{\varphi}(10,\omega)$ and the normal derivative $H_{x_2}(x,\omega) = \tilde{\psi}(10,\omega)$ as a function of $f = \dfrac{\omega}{2\pi}$, just above the target at $x = (10, 0)$ on the air-soil interface. Despite the scatter in the noisy data, the C^2 cubic spline smoothing process appears to be doing a good job of returning smoothed values close to the original. The largest differences are around the peaks of the curves and to the far left of Figure 3. Figure 4 displays the real part of $H(x,\omega_0) = \tilde{\varphi}(x,\omega_0)$ along the air-soil interface $\{x_2 = 0\}$ for $\omega_0 = 1.0 \cdot 2\pi$ GHz. It should be clarified, that smoothing was done for each spatial point $x = x_{1i}$, where $x_{1i} = -L_{x_1} + \triangle_{x_1}(i - 1/2), i = 1.\cdots, M_{x_1}$, with respect to the frequency ω as described above. However, no smoothing was performed with respect to the spatial variable x_1.

In this first test the p and H imaging algorithms were applied to a single target of circular shape filled with TNT as specified above. The results used data over frequencies from 0.5 GHz to 3 GHz, using an increment of $\triangle f = .01\ GHz$. The stopping criteria

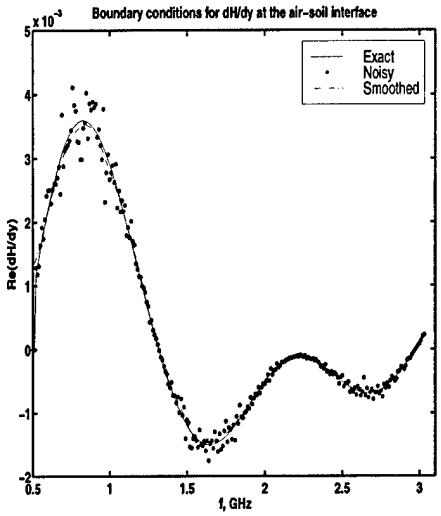

Figure 3: $\mathrm{Re}[H_{x_2}(x,\omega)]$ as a function of the frequency f at $x = (10, 0)$.

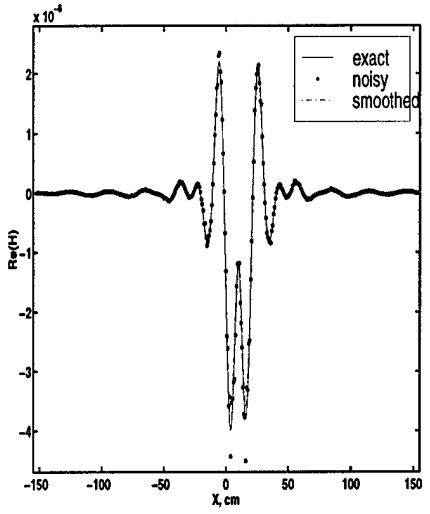

Figure 4: $\mathrm{Re}[H(x_1,\omega)]$ for $\omega_0 = 1.0 \bullet 2\pi GHz$ as a function of x_1 along $\{x_2 = 0\}$.

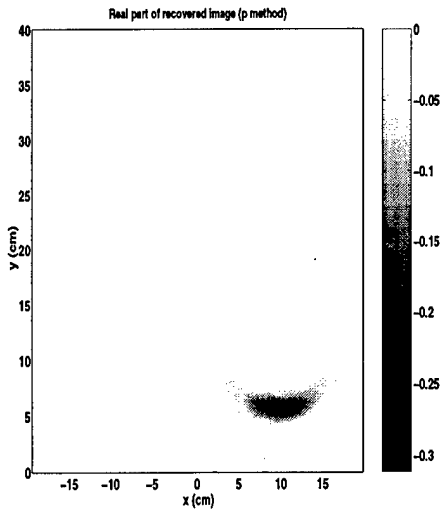

Figure 5: $\mathrm{Re}[h_{imaged}(x)]$ for the solution of the inverse problem by the p method.

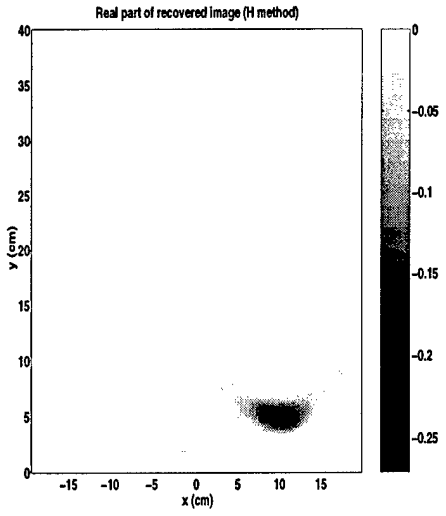

Figure 6: $\mathrm{Re}[h_{imaged}(x)]$ for the solution of the inverse problem by the H method.

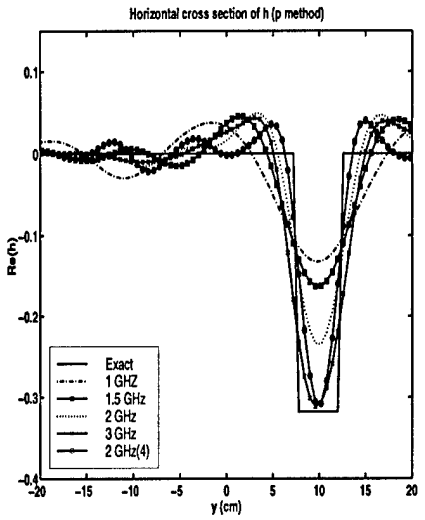

Figure 7: Horizontal cross-section of $\mathrm{Re}[h_{imaged}(x)]$ after two sweeps using the p method for different values of $\omega_{\max}$.

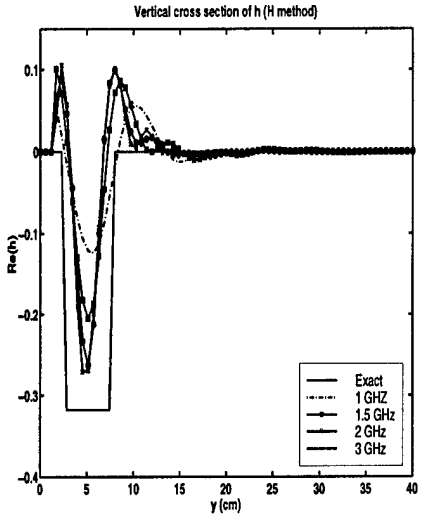

Figure 8: Horizontal cross-section of $\mathrm{Re}[h_{imaged}(x)]$ after two sweeps using the H method for different values of $\omega_{\max}$.

here and elsewhere requires running one more sweep than was used, stopping when the last result either decreased, showed significant oscillations or changed very little. Figures 5 and 6 display the real part of the imaged function $h := h_{imaged}(x_\alpha)$ obtained after two sweeps of the p-method and one sweep of the H-method respectively. The contour plots of the recovered function $\mathrm{Re}(h)$ are similar, both accurate as to the centered location, both lacking significant artifacts. However, the maximal value of the H solution within the target is about 20% off the correct one. Whereas the value for the p solution is exact. This difference speaks favorably for p solution in the light of the goal of diagnostics of mine-like targets. The imaginary part of h here and elsewhere is in general less satisfactory because $|\mathrm{Im}\,(k)| << |\,\mathrm{Re}(k)|$ by Table 1.

The effects of using frequencies from $f_{\min} = 0.5\ GHz$ to various upper values of $f_{\max}$ from 1.0 GHz to 3.0 GHz was also considered for both the H and p methods. The frequency spacing $\triangle f$ is fixed at 0.01 GHz. To clearly demonstrate the results quantitatively, cross-sections of the real part of the imaged function h along both vertical and horizontal lines are displayed for each method. In each case, the cross section is along the line where the values are greatest. Typically for the horizontal lines this is close to $x_2 = 5\ cm$, and for the vertical lines close to $x_1 = 10\ cm$. In Figures 7-10 the solid lines represent the exact values and various other lines, as identified by the legend, the cross sections of various computed solutions.

As one can see, the increase of the range of the frequencies from $0.5 - 1\ GHz$ to $0.5 - 1.5$ GHz to $0.5 - 2\ GHz$ gives significant improvements in the heights of the recovered images

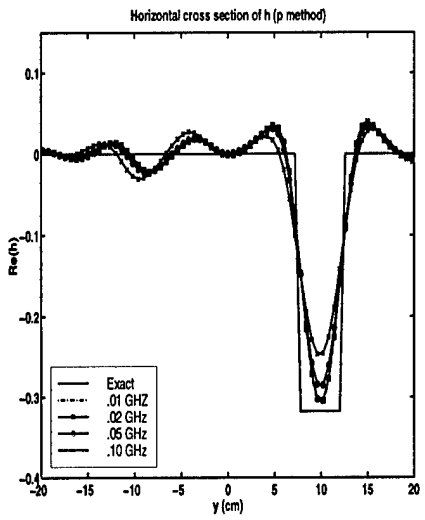

Figure 9: Vertical cross-section of $\mathrm{Re}[h_{imaged}(x)]$ after two sweeps using the p method for different values of $\omega_{\max}$.

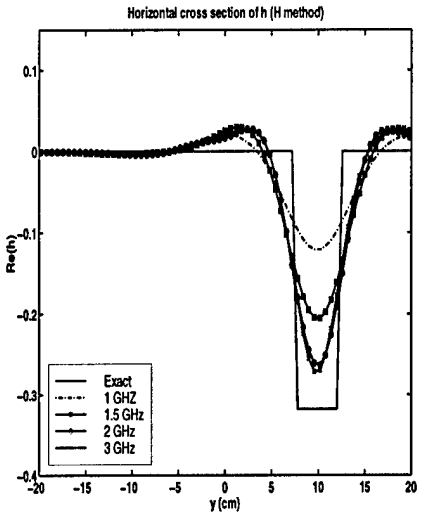

Figure 10: Vertical cross-section of $\mathrm{Re}[h_{imaged}(x)]$ after two sweeps using the H method for different values of $\omega_{\max}$.

for both the p- and H-methods and is thus clearly desirable.

The effect of various frequency spacing $\triangle f = \triangle\omega/2\pi$ was also examined. It was concluded that it is unnecessary to use a fine frequency spacing of $\triangle f = 0.01\ GHz$, since $\triangle f = 0.02\ GHz$ provided the same results.

5.4.2 Three targets filled with TNT

In the remaining numerical examples the application of both algorithms to the case of three multiple mine-like targets of different sizes and soil depths is considered. These targets are again in wet soil with a 5% moisture content and filled with TNT, using parameter values from Table I. The buried objects chosen for this test are three rectangular mine-like targets. Two of the targets are $5 \times 4\ cm$ and the third is $10 \times 4\ cm$. Three mine-like targets were examined to see if the H and p inversion algorithms could separate multiple scatterers and reconstruct well the deeper object. The frequency range in this test is from 0.5 to 3.0 GHz for the p method and from 0.5 to 2.0 GHz for the H method, and the frequency step is $\triangle f = 0.02\ GHz$ as suggested above. The two smaller targets are centered 5 cm into the ground and the larger rectangular target is centered 10 cm deep into the ground. The horizontal centers are at $-10, 0$ and 10 cm. As in the first example, the detector readings are simulated from the forward problem with the addition of $\sigma = .10$ multiplicative Gaussian noise.

The real part of the corresponding function $h(x)$ is displayed in Figure 11. The reconstructed images of the real part of the coefficient are shown in Figures 12-14. From these

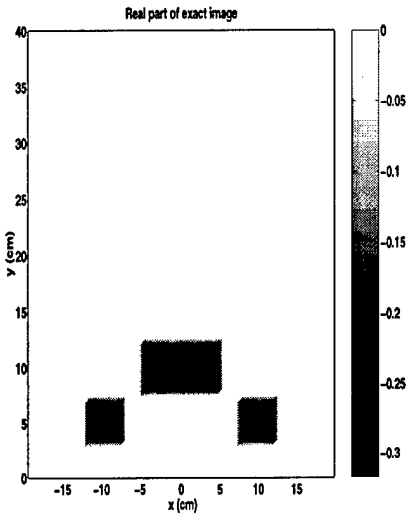

Figure 11: Re$[h(x)]$ for three mine-like targets of various sizes.

figures it can be seen that both algorithms perform reasonably well. The locations and shapes of the objects are both fairly accurate. The methods provide maximal values of Re$[h_{imaged}(x)]$ within targets which are about 12% off the target value for p-method and 7% off for H-method.

5.4.3 Conclusions for Comparison of p and H Methods.

The H-method generally works better for the lower upper frequency than the p-method. Also, unlike p-method, H-method does not require neither the differentiation of the data with respect to the frequency, nor independence of the loss tangent from the frequency, which might be an advantage for the case of an experimental data. Both methods provide accurate locations of targets. Another *key* parameter for the goal of diagnostics of mine-like targets is the maximal value of Re$[h_{imaged}(x)]$ within targets. In the case of a single target, which is the most important one for a practical scenario, the p-method provides very accurate maximal values of Re$[h_{imaged}(x)]$ within a target, as opposed to the H-method, for which those values are 20% off the correct ones. The latter speaks favorably for the p-method in the light of the above diagnostics goal.

As to the comparison with the best algorithm in the field, H-method is an *advanced* version of the original algorithm of F. Natterer **[5,6,19]**. In those works only diagonal elements of resulting matrices to be inverted were counted, as opposed to our case, in which the entire matrix is counted. Therefore, if we would literally follow the idea of Natterer by counting only diagonal elements of those matrices in the above H method, then images would be much worse than those obtained above.

5.5. CONCLUSIONS

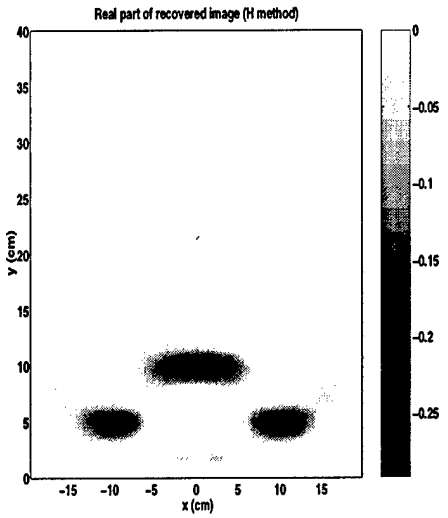

Figure 12: Final reconstruction of $\mathrm{Re}[h_{imaged}(x)]$ after one sweep using the p method.

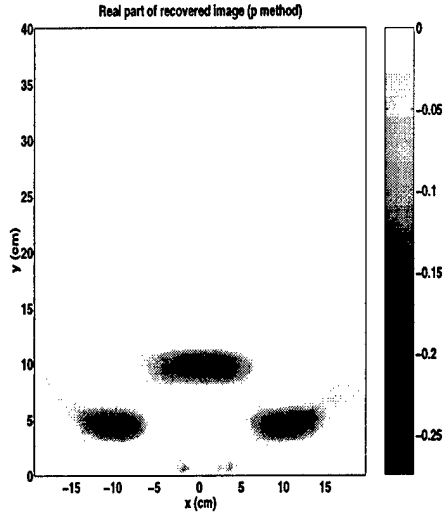

Figure 13: Final reconstruction of $\mathrm{Re}[h_{imaged}(x)]$ after one sweep using the H method.

The problem of differentiating mines from clutter using hand-held GPR was considered as an inverse problem. In this approach locations and electrical properties of mine-like targets would be imaged via solution of an inverse problem. The input data for such a problem would be the back-reflected electrical signal measured at many frequencies ranging from 0.5 to 3 GHz. Locations and electrical properties of targets, in turn might be used on a later stage as an input for a procedure of classification of targets.

Three major tasks were achieved in this project. Each of these required about one year of effort. First, a new rapid algorithm for the solution of the forward problem on high frequencies was developed and implemented [1,3]. This task, though axillary, was necessary to perform, because the conventional classical algorithm of Gaussian elimination is too slow for this range of frequencies.

Next, a second generation of the Elliptic Systems Method (ESM), which was used earlier in Diffusion Tomography, was developed and tested for the inverse problem of diagnostics of mine-like targets using GPR [2] (p-method). The key new element of this second generation method is that the resulting integro-differential equation is solved directly, rather than by eliminating integrals, as it previously was. In addition, a fast preconditioner was developed for the Conjugate Gradient Method, which significantly speeded up solutions of inverse problems of this project. The resulting algorithm provides accurate images of both locations of targets and values of the $\mathrm{Re}[h_{\ imaged}\ (x)]$ within them in about 6 minutes of CPU time on a SGI Origin 200 with a single processor. This timing is well acceptable for the goal of diagnostics of mine-like targets, since the process of diagnostics is much slower than one of screening. Still, this timing can well be decreased by a factor of five, if using fast dual precessing techniques.

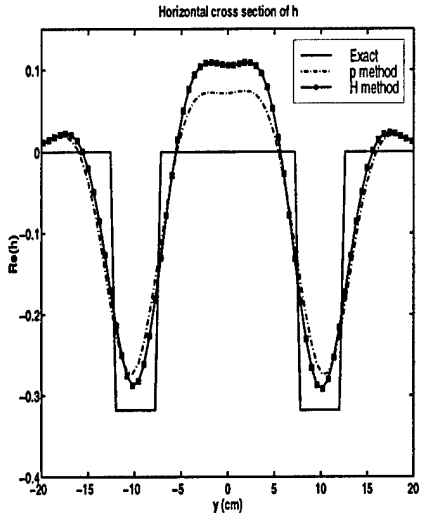

Figure 14: Horizontal reconstruction of Re$[h_{imaged}(x)]$ using the p and H methods.

Finally, a modified version of the algorithm [2] was developed (H-method), which is actually an advanced variant of the method of a well known German scientist F. Natterer [19]. It was shown that both versions provide the same accurate locations of targets, while the second version usually performs better for the lower values of the upper frequency. However, in the practically most important case of a single target the first version performs much better for the key parameter Re$[h_{\ imaged}\ (x)]$ within the target. It is also reasonable to conclude that if using the original method of [19], in which only diagonal elements of matrices are counted (as opposed to its more advanced version used here), the quality of the resulting images would be much worse than ones presented above. This speaks in favor of the second generation of the ESM, as compared with the best competing technique of F. Natterer.

5.6 POSSIBLE FUTURE DIRECTION OF RESEARCH

First, it would be very interesting to verify the performance to both p- and H-methods on the experimental data. The methods are now mature, although a few new features should be implemented before this would be possible. Some of these features are: the measurement line should be "raised" from the air/ground interface, geometric irregularities of the air/ground interface need to be incorporated in the model, and possibly a point source, as opposed to the current initializing plane wave, should be incorporated.

There is also a second pressing need of research, connected with the development of globally convergent, as opposed to locally convergent, inverse algorithms for imaging of land targets. This would be a far advanced second generation of the above methods. The vast majority of inverse techniques, including the ones presented above, is heavily relying on an assumption that the properties of soil are known with a good accuracy. This leads either to the linearization of the inverse problem, or to a perturbation approach, which is a slight

modification of the linearization. In practice, however, electrical properties of soil are not always known with a good accuracy. Therefore linearization of an inverse problem is not feasible in such cases. The key drawback of the conventional least squares objective functions is that they suffer from the problem of local minima, as soon as the starting vector is chosen far from the solution [**18**]. Therefore, in the scenarios when properties of soil are not known with a good accuracy, there is a pressing need for algorithms, which would neither rely on the perturbation approach, nor suffer from the problem of local minima.

A new idea of globally convergent algorithms has been developed by M. V. Klibanov in the past several years, cf. [**17**]. It was only recently however, when the computational feasibility of this idea was verified by M. V. Klibanov and A. Timonov [**18**]. In [**18**], this approach was termed *convexification.* By the convexification approach, the original inverse problem is reduced first to a boundary value problem for a non-linear integro differential equation, in which the unknown coefficient is not involved. This equation is similar to the above equation (5.8a), except of the non-linearity, which is obviously not present in (5.8a). Next, this boundary value problem is solved via a least squares cost functional J. The key new element of J, however, is the presence of the so-called *Carleman weight function (CWF).* The role of the CWF is that it guarantees strict convexity of J on a compact set of user's choice. Actually, the role of the CWF is to suppress the presence of terms with low order derivatives, which are responsible for destroying the strict convexity of the Laplace operator $\bigtriangledown^2$. Therefore, because of strict convexity, rapid global convergence of a number of minimization algorithms to the unique minimizer of J is guaranteed. If can be also proven that the distance between the minimizer of J and the vector, which corresponds to the correct solution of the inverse problem, is small, if the data are not "too noisy". Preliminary results in this direction are quite promising.

6. LISTING OF ALL PUBLICATIONS AND TECHNICAL REPORTS SUPPORTED BY THIS GRANT

A. Papers published in peer-reviewed journals

1. Yu. A. Gryazin, M. V. Klibanov, and T. R. Lucas, GMRES computation of high frequency electrical field propagation in land mine detection, *Journal of Computational Physics,* 158, 98-115, 2000.

2. Yu. A. Gryazin, M. V. Klibanov, and T. R. Lucas, Numerical solution of a subsurface imaging inverse problems, *SIAM Journal on Applied Mathematics*, to appear in 2001.

B. Papers published in non-peer-reviewers journals or in conference proceedings

3. Yu. A. Gryazin, M. V. Klibanov, and T. R. Lucas, Tomographic images of land mines by the elliptic systems method using GPR: Efficient solution of the forward problem, *Proc. of SPIE "Detection and Remediation Technologies for Mines and Minelike Targets IV",* 3710, 875-886, 1999.

4. T. P. Weldon, Yu. A. Gryazin and M. V. Klibanov, Comparison of 2D and 1D approaches to forward problem in mine detection, *Proc. of SPIE "Detection and Remediation Technologies for Mines and Minelike Targets V",* 4038, 1171-1179, 2000.

5. Yu. A. Gryazin and M. V. Klibanov, Solution of inverse problems of mine detection by the elliptic systems method, *Proc. of SPIE "Detection and Remediation Technologies for Mines and Minelike Targets V",* 4038, 1140-1148, 2000.

C. Papers presented at meetings, but not published in conference proceedings

6. T. P. Weldon, Yu. A. Gryazin and M. V. Klibanov, Novel inverse methods in land mines imaging, *IEEE International Conference on Acoustics, Speech and Signal Processing,* Salt Lake City, Utah, 7-11 May, 2001; this paper can be found on

   http://www2.uncc.edu/tpw/papers/papers.html.

   7. M. V. Klibanov, Y.A. Gryazin, and T.R. Lucas, Method of integro-differential PDEs for imaging of land mines, *SIAM Annual Meeting,* San Diego, CA 2001.

   8. T.R. Lucas and Yu.A. Gryazin, Preconditioning technique in land mines imaging, *SIAM Annual Meeting*, San Diego, CA 2001.

   9. T.R. Lucas, Yu.A. Gryazin, and M.V. Klibanov, Second generation of Elliptic Systems Method for Land Mine Detection and Diffusion Tomography, *SIAM Annual Meeting*, Puerto Rico, 2000.

10. T.R. Lucas, Yu.A. Gryazin, and M.V. Klibanov, Identification of anipersonnel land mines by a new algorithm in inverse problems, National Radio Science Meeting, Boulder, CO 2001.

11. T.R. Lucas and Yu.A. Gryazin, A new approach to interior coefficient recovery in subsurface scattering and diffusion tomography, *International Conference On Applied Inverse Problems*, Montecatini Terme, Italy, 2001.

D. Manuscripts submitted, but not yet published

12. Yu. A. Gryazin, M. V. Klibanov, and T. R. Lucas, Two novel numerical methods for an inverse problem for the 2-D Helmholtz equation, submitted to *Journal of Computational Physics* in August 2001.

E. Technical reports submitted to ARO

Three interim annual reports were submitted to ARO, each of which has the same title as the title of this grant, i.e., "A Novel Principle for Data Processing from Hand-Held Ground Penetrating Radars":

1. First interim report. Date of submission: March 1999. Dates covered: 7/1/98 - 12/31/98.
2. Second interim report. Date of submission: March 2000. Dates covered: 1/1/99 - 12/31/99.
3. Third interim report. Date of submission: March 2001. Dates covered: 1/1/00 - 12/31/00.

7. LIST OF ALL PARTICIPATING SCIENTIFIC PERSONEL

This grant has provided support for the following people:

1. Michael V. Klibanov, Principal Investigator, Ph.D., Professor, Department of Mathematics, University of North Carolina at Charlotte.

2. Thomas R. Lucas, Co-Principal Investigator, Ph.D., Professor, Department of Mathematics, University of North Carolina at Charlotte.

3. Yuriy A. Gryazin, Senior Researcher, Ph.D., Department of Mathematics, University of North Carolina at Charlotte (at that time). Currently with the Department of Mathematics of the Idaho State University.

4. Sergey Pamyatnikh, Doctoral Student (Thesis Advisor M. V. Klanbov), Department of Mathematics, University of North Carolina at Charlotte.

5. Vipal J. Patel, then Graduate Student of Masters program of Electrical Engineering Department, University of North Carolina at Charlotte. Mr. Patel earned his Masters degreee in Electrical Engineering while supported by this grant. His Thesis Advisor was Thomas P. Weldon, Ph.D., Assistant Professor of the same department.

8. REPORT ON INVENTIONS

None.

10. BIBLIOGRAPHY

1. C. de Boor, *A Practical Guide to Splines*, Springer-Verlag, New York, 1978.

2. N. V. Budko and P. M. van den Berg, Characterization of a two-dimensional subsurface object with an effective scattering model, *IEEE Trans. on Geosci. and Remote Sensing*, 37, 2585-2596, 1999.

3. M. Cheney and D. Isaacson, Inverse problems for a perturbed dissipative half-space, *Inverse Problems*, 11, 865-888, 1995.

4. L. M. Delves and J. L. Mohamed, *Computational Methods For Integral equations*, Cambridge University Press, Cambridge, 1985.

5. O. Dorn, H. Bertete-Aguirre, J. G. Berrymon, and G. C. Paparicolaou, A nonlinear inversion method for 3D electromagnetic imaging using adjoint fields, *Inverse Problems,* 15, 1523-1558, 1999.

6. O. Dorn, E. L. Miller, and C. M. Rappaport, A shape reconstruction method for electromagnetic tomography using adjoint fields and level sets, *Inverse Problems*, 16, 1119-1156, 2000.

7. a. *Dielectric Constant and Loss Tangent of Explosives; b. Permittivity and Conductivity vs. Frequency for Sandy Loam for Various Moistures*, data of U.S. Army Belvoir RD&E Center (unpublished).

8. A. George and J. W.-H. Liu, *Computer Solution of Large Sparse Positive Definite Systems*, Prentice-Hall, Inc., Englewood Cliffs, New Jersey, 1981.

9. W. H. Hayt, *Engineering Electromagnetics*, McGraw Hill, 3rd ed., 1974.

10. Yu. A Gryazin, M. V. Klibanov, and T. R. Lucas, Imaging the diffusion coefficient in a parabolic inverse problem in optical tomography, *Inverse Problems*, 15, 373-397, 1999.

11. T. Kato, *Perturbation Theory For Linear Operators*, Springer-Verlag, New York, 1966.

12. M. V. Klibanov, T. R. Lucas and R. M. Frank, A fast and acurate imaging algorithm in optical/diffusion tomography, *Inverse Problems*, 13, 1341-1361, 1997.

13. M. V. Klibanov, T. R. Lucas, Elliptic systems method in diffusion tomography using back-reflected data, *Inverse Problems*, 16, 199-221, 2000.

14. M. V. Klibanov and T. R. Lucas, Numerical solution of a parabolic inverse problem in optical tomography using experimental data, *SIAM J. Appl. Math.*, 59, 1763-1789, 1999.

15. M. V. Klibanov and F. Santosa, Computational quasi-reversibility method for Cauchy problems for Laplace's equation, *SIAM J. Appl. Math.*, 51, 1655-1675, 1991.

16. R. Lattes and J.-L. Lions, *Method of Quasi-Reversibility: Applications to Partial Differential Equations*, Elsevier, New York, 1969.

17. M. V. Klibanov, Global convexity in a three-dimensional inverse acoustic problem, *SIAM Journal on Math. Anal.,* 28, 1371-1378, 1997.

18. M. V. Klibanov and A. Timonov, A new slant on inverse problems of electromagnetic frequency sounding: "Convexification" of a multi-extremal objective function via Carleman weight function, *Inverse Problems*, 17, 2001, to appear.

19. F. Natterer and F. Wuebbeling, A propagation-backpropagation method for ultrasound tomography, *Inverse Problems,* 11, 1225-1232, 1995.